Downloaded from rnajournal.cshlp.org on April 26, 2024 - Published by Cold Spring Harbor Laboratory Press

Structural and biochemical characterization of CRN-5 and Rrp46: An exosome component participating in apoptotic DNA degradation

CHE-CHUAN YANG,[1,2] YI-TING WANG,[2,3,4] YU-YUAN HSIAO,[2,4] LYUDMILA G. DOUDEVA,[2] PAN-HSIEN KUO,[2,4] SIH YAO CHOW,[2] and HANNA S. YUAN[1,2,3]

[1]Graduate Institute of Biochemistry and Molecular Biology, National Taiwan University, Taipei, 10617 Taiwan, Republic of China
[2]Institute of Molecular Biology, Academia Sinica, Taipei 11529, Taiwan, Republic of China
[3]Taiwan International Graduate Program, Institute of Chemical Biology and Molecular Biophysics, Academia Sinica, Taipei 11529, Taiwan, Republic of China
[4]Institute of Bioinformatics and Structural Biology, National Tsing Hua University, Hsinchu, Taiwan 30013, Republic of China

ABSTRACT

Rrp46 was first identified as a protein component of the eukaryotic exosome, a protein complex involved in 3′ processing of RNA during RNA turnover and surveillance. The Rrp46 homolog, CRN-5, was subsequently characterized as a cell death-related nuclease, participating in DNA fragmentation during apoptosis in *Caenorhabditis elegans*. Here we report the crystal structures of CRN-5 and rice Rrp46 (oRrp46) at a resolution of 3.9 Å and 2.0 Å, respectively. We found that recombinant human Rrp46 (hRrp46), oRrp46, and CRN-5 are homodimers, and that endogenous hRrp46 and oRrp46 also form homodimers in a cellular environment, in addition to their association with a protein complex. Dimeric oRrp46 had both phosphorolytic RNase and hydrolytic DNase activities, whereas hRrp46 and CRN-5 bound to DNA without detectable nuclease activity. Site-directed mutagenesis in oRrp46 abolished either its DNase (E160Q) or RNase (K75E/Q76E) activities, confirming the critical importance of these residues in catalysis or substrate binding. Moreover, CRN-5 directly interacted with the apoptotic nuclease CRN-4 and enhanced the DNase activity of CRN-4, suggesting that CRN-5 cooperates with CRN-4 in apoptotic DNA degradation. Taken together all these results strongly suggest that Rrp46 forms a homodimer separately from exosome complexes and, depending on species, is either a structural or catalytic component of the machinery that cleaves DNA during apoptosis.

Keywords: RNA turnover; DNA degradation; crystal structure; RNase PH; RNase; DNase; apoptotic nuclease

INTRODUCTION

A conserved family of RNase phosphorolysis (PH) proteins plays a key role in the correct processing, quality control, and turnover of cellular RNA molecules and is critical to the precise expression of genetic information and cell survival (Symmons et al. 2002). Most of the RNase PH family proteins have 3′-to-5′ exoribonuclease activity, capable of removing the 3′-end nucleotide by adding a phosphate, rather than a water molecule, to the cleaved phosphodiester bond, and are therefore involved in phosphorolytic RNA processing and degradation. Examples include the prokaryotic PNPase (Littauer and Grunberg-Manago 1999) and RNase PH (Deutscher et al. 1988), and the archaeal exosome (Evguenieva-Hackenberg et al. 2003).

Rrp46 is an RNase PH family protein and was first identified as a component protein of the eukaryotic exosome, a multiprotein complex involved in RNA processing, surveillance, and turnover of various pre-mRNA, mRNA, snRNA, snoRNA, rRNA, and tRNA species in the cytoplasm and the nucleus (Anderson and Parker 1998; de la Cruz et al. 1998; Allmang et al. 1999a; van Hoof et al. 2000; Hilleren et al. 2001; Suzuki et al. 2001; Torchet et al. 2002; Mitchell and Tollervey 2003; Kadaba et al. 2004; Raijmakers et al. 2004). The yeast exosome core consists of six RNase PH family proteins (Rrp41, Rrp42, Rrp43, Rrp45, Rrp46, and Mtr3), three KH-domain-containing proteins (Rrp4, Rrp40, and Csl4), and additional hydrolytic exoribonucleases (Rrp44/Dis3 and Rrp6) (Mitchell et al. 1997; Allmang et al. 1999b). Related exosomes have been described in other species, such as among the hyperthermophilic archaea,

Reprint requests to: Hanna S. Yuan, Institute of Molecular Biology, Academia Sinica, Taipei 11529, Taiwan, Republic of China; e-mail: hanna@sinica.edu.tw; fax: 886-2-27826085.

Article published online ahead of print. Article and publication date are at http://www.rnajournal.org/cgi/doi/10.1261/rna.2180810.

Downloaded from rnajournal.cshlp.org on April 26, 2024 - Published by Cold Spring Harbor Laboratory Press

nematodes, unicellular parasites, flies, plants, and humans (Allmang et al. 1999b; Chekanova et al. 2000; Estevez et al. 2001; Koonin et al. 2001; Andrulis et al. 2002; Evguenieva-Hackenberg et al. 2003; Liu et al. 2006). Although most cells have other enzymes that can degrade RNA, the exosome components are essential for cell survival (Allmang et al. 1999b; van Dijk et al. 2007).

The six RNase PH family proteins in the human exosome—namely, hRrp41, hRrp42, hRrp43, hRrp45, hRrp46, and hMtr3—form a ring-like hexamer structure as revealed by the crystal structure analysis of the exosome core (Liu et al. 2006). A similar structural organization is observed in the archaeal exosome core complex, in which the two archaeal RNase PH family proteins, Rrp41 and Rrp42, form a hexameric ring composed of three copies of Rrp41–Rrp42 heterodimers (Buttner et al. 2005; Lorentzen and Conti 2005; Lorentzen et al. 2005; Navarro et al. 2008). The phosphorolytic exonuclease active sites of the archaeal exosome are situated in the internal "processing chamber" of the Rrp41–Rrp42 ring. Only Rrp41 has an RNase active site, whereas Rrp42 is required for complex assembly and activity (Buttner et al. 2005; Lorentzen and Conti 2005; Lorentzen et al. 2005; Navarro et al. 2008). On the other hand, the recombinant yeast and human exosome cores are inactive and lack any detectable phosphorolytic exoribonuclease activity, suggesting that all of the RNase PH proteins in the ring, including hRrp46, are inactive (Liu et al. 2006). Only when associated with Rrp44/Dis3 does the yeast exosome have hydrolytic activity (Dziembowski et al. 2007; Bonneau et al. 2009; Schaeffer et al. 2009). Interestingly, the exosome core in the plant lineage seems to have phosphorolytic activity (Chekanova et al. 2000), indicating that eukaryotic exosomes may have evolved divergent means of RNA degradation.

hRrp46 is also named CML28, as it is a 28-kDa antigen abundant in the sera of chronic myelogenous leukemia (CML) patients after allogeneic hematopoietic stem cell transplantation (Wu et al. 2000). Additional characterization showed that CML28 is highly expressed in a variety of cancer cells and tissues, including leukemia, lung cancer, and prostate cancer (Yang et al. 2002). hRrp46/CML28 has therefore been further evaluated as an immunotherapy target for the stimulation of anti-tumor immune response (Zhou et al. 2006; Xie et al. 2008). Intriguingly, autoantibodies against hRrp46, and the exosome component protein PM-Scl100, are often found in patients with autoimmune diseases, including scleroderma, polymyosistis/sclerodema overlap syndrome, and idiopathic inflammatory myopathy (Reichlin et al. 1984; Bluthner and Bautz 1992; Ge et al. 1992; Brouwer et al. 2002). It is not clear why hRrp46 or antibodies against hRrp46 are highly expressed in cancers and autoimmune diseases, but these results do hint, albeit vaguely, at a connection between hRrp46 expression and cell survival.

The *Caenorhabditis elegans* Rrp46 homolog, CRN-5, was further identified as a cell death-related nuclease involved in DNA fragmentation during apoptosis (Parrish and Xue 2003). CRN-5 shares significant sequence identity (31%) with human hRrp46 (see the sequence alignment in Fig. 1). RNAi knockdown of CRN-5 resulted in an increase of TUNEL-reactive cells and the delayed appearance of embryonic cell corpses during development in *C. elegans*, indicating the involvement of CRN-5 in apoptotic DNA degradation (Parrish and Xue 2003). Moreover, CRN-5 can also form another complex, the degradeosome, with CPS-6, WHA-1, CYP-13, and a number of CRN nucleases, including CRN-4 and CRN-1 (Parrish and Xue 2003). This result implies that CRN-5 may not be associated with the exosome when it is involved in DNA fragmentation during apoptosis.

To understand how Rrp46/CRN-5 functions in apoptotic DNA fragmentation, we characterized the biochemical properties of *C. elegans* CRN-5 and compared them to those of human hRrp46 and rice oRrp46. We also determined the crystal structures of CRN-5 and oRrp46. Our results show that both recombinant and endogenous Rrp46/CRN-5 are homodimers. Rice oRrp46 has phosphorolytic RNase activity and hydrolytic DNase activity. Mutational studies of oRrp46 verified the residues involved in catalysis and substrate binding. On the other hand, the recombinant hRrp46 and CRN-5 have no detectable RNase and DNase activity. Crystal structural comparison of the active oRrp46 versus the inactive hRrp46 further suggests the structural basis for the enzyme activity, where only the active oRrp46 has basic residues appropriate for RNA binding. Moreover, CRN-5 binds to DNA and to the apoptotic nuclease CRN-4 and thereby promotes the DNase activity of the apoptotic nuclease CRN-4 (Hsiao et al. 2009), suggesting that CRN-5 is involved in DNA degradation. Our findings therefore suggest that Rrp46 is a dual-function protein: when associated with the exosome, it is involved in RNA processing and turnover in normal cells, and when it forms a homodimer it is involved in DNA degradation during apoptosis. This finding therefore provides a new direction for the study of the role of hRrp46 in cancer and autoimmune diseases.

RESULTS

Rrp46 forms a stable homodimer

The cDNA encoding *C. elegans* CRN-5, rice (*Oryza sativa*) oRrp46, and human hRrp46 were PCR-amplified and cloned into His-tagged fusion constructs. Recombinant Rrp46/CRN-5 proteins were overexpressed in *Escherichia coli* and purified by chromatographic methods. The His-tagged oRrp46 and hRrp46 were purified to a homogeneity of >98%, whereas CRN-5 was less homogeneous with a partial population of cross-linked dimers as shown by

Downloaded from rnajournal.cshlp.org on April 26, 2024 - Published by Cold Spring Harbor Laboratory Press

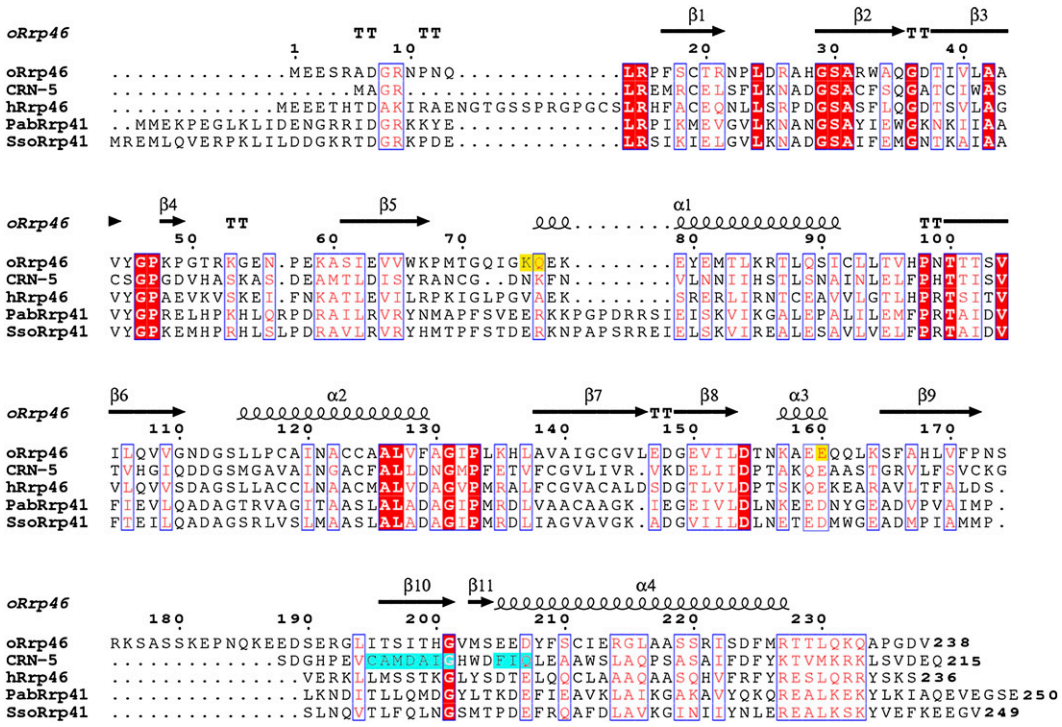

FIGURE 1. Sequence alignment of rice, human, and *C. elegans* Rrp46 (CRN-5) and archaeal Rrp41. Eukaryotic Rrp46 shares significant sequence identity with archaeal Rrp41. Sequences listed here are Rrp46 from *Oryza sativa* (oRrp46), *Caenorhabditis elegans* (CRN-5), and human (hRrp46), and Rrp41 from *P. abyssi* (PabRrp41) and *S. solfataricus* (SsoRrp41). The secondary structure generated from the crystal structure of oRrp46 is shown above the sequence. TT represents β-turns. Identical and similar residues are shown in red. Mutational residues constructed in this study are shown in yellow. The residues involved in homodimeric interactions in CRN-5 are shown in cyan. The alignment was generated by ClustalW (http://www.ch.embnet.org/software/ClustalW.html) and ESpript (Gouet et al. 2003).

SDS-PAGE in a reduced condition (see Fig. 2A). Mass spectrometry verified the correct molecular weight of each protein (data not shown) (theoretical molecular weights for the recombinant proteins: 26,974 Da for oRrp46; 24,988 Da for CRN-5; and 27,412 Da for hRrp46). The three proteins share high sequence identity: 35% between hRrp46 and oRrp46, 31% between hRrp46 and CRN-5, and 28% between oRrp46 and CRN-5 (see Fig. 1).

The three purified proteins, CRN-5, oRrp46, and hRrp46, eluted with a size between 44 kDa and 75 kDa in size-exclusion chromatography under reduced conditions (1 mM β-mercaptoethanol) (Fig. 2B). The molecular weights of the three proteins estimated by dynamic light scattering (DLS) and analytical ultracentrifugation (AUC) under reduced conditions were also in the range of 42– 59 kDa (Fig. 2C,D), suggesting that the recombinant proteins were homodimers with molecular weights of ~50 kDa. To further verify that Rrp46 forms homodimers in a cellular environment, endogenous Rrp46 in the cell extracts of human 293T cells and rice callus were blotted using antibodies against hRrp46 and oRrp46 after gel filtration fractionation (Fig. 2E). Two populations of hRrp46 were observed at different elution volumes with or without the addition of the reducing agent (1 mM β-mercaptoethanol): the first peak eluted at 45–60 mL, indicating a high-molecular-weight complex, and the second peak appeared at 80–85 mL, indicating a mixture of a dimer and a monomer. The cell extract of rice callus gave similar results that oRrp46 migrated as a large-size complex and a small-size dimer. As a control, the 293T cell extract eluted from gel filtration fractionation was also blotted with antibodies against hRrp42, one of the six RNase PH family proteins in the exosome core. The Western blot displayed in Figure 2E shows that hRrp42 only eluted in a complex with a molecular weight >158 kDa. The complex identified by anti-hRrp42 overlapped with the complex indicated by probing with anti-hRrp46, suggesting that both proteins were likely associated with the same complex, the exosome. This result is consistent with the previous result in the reconstitution of the human exosome in which a monodisperse peak with a molecular weight of ~400 kDa and a smaller size peak were observed in the gel filtration under low-salt conditions (Liu et al. 2006). In summary, these results suggest that the exosome component protein hRrp42 is associated with a protein complex, but it does not form a monomer or a dimer in cells. On the other hand, the endogenous Rrp46 is associated with a protein complex and it also forms a separate dimer in a cellular environment.

Downloaded from rnajournal.cshlp.org on April 26, 2024 - Published by Cold Spring Harbor Laboratory Press

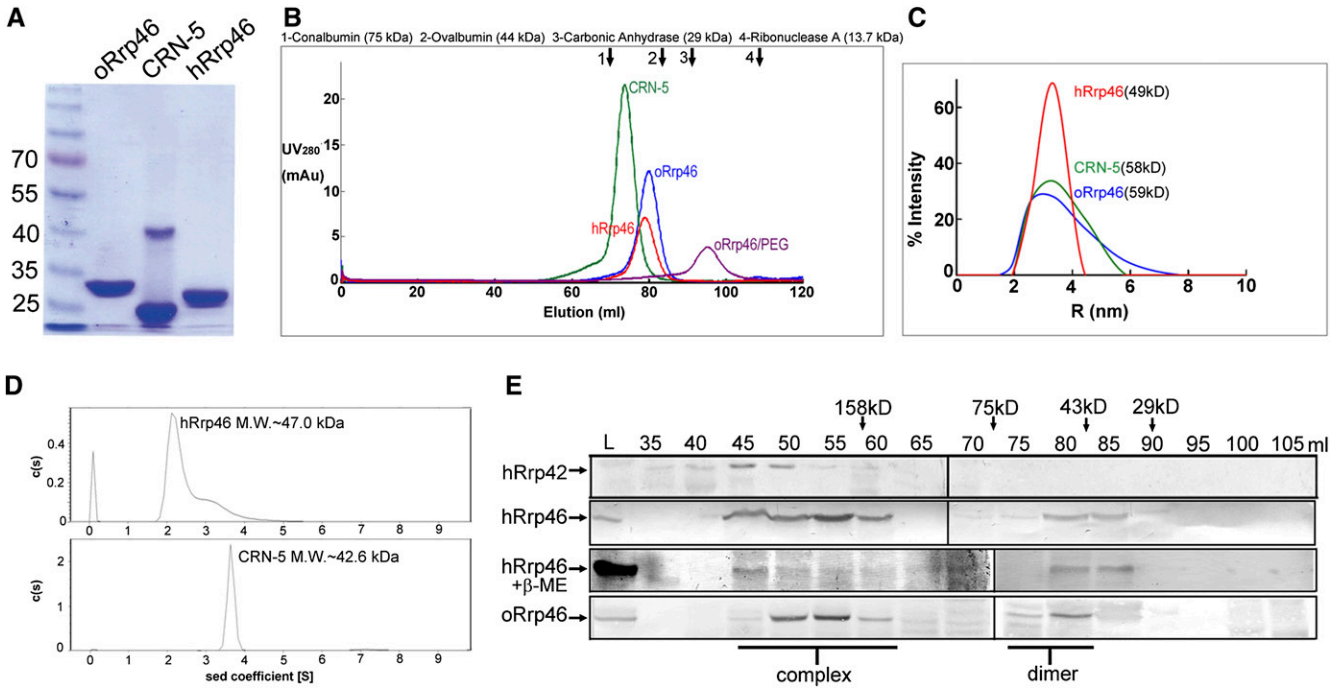

FIGURE 2. Recombinant and endogenous Rrp46/CRN-5 are dimeric proteins. (*A*) The purified recombinant Rrp46 proteins from different species were analyzed by SDS-PAGE. CRN-5 was less homogeneous with strong linked dimers that could not be dissociated into monomers on SDS-PAGE under the reduced condition. Molecular weight markers are shown as indicated. (*B*) Gel filtration (Superdex 200) profiles for hRrp46, oRrp46, and CRN-5. The recombinant Rrp46/CRN-5 all eluted with a size of a homodimer in a buffer of 25 mM Tris-HCl (pH 7.6), 150 mM NaCl and 1 mM β-mercaptoethanol. oRrp46 shifted into monomers with the addition of 5% PEG 3350 (oRrp46/PEG). (*C*) Dynamic light scattering (DLS) analysis of native Rrp46 proteins. The estimated molecular weights of each protein (in parentheses) are listed in the figure. (*D*) Analytical ultracentrifugation (AUC) of recombinant hRrp46 and CRN-5. The sedimentation velocities of hRrp46 and CRN-5 were recorded in a buffer of 25 mM Tris-HCl (pH 7.6), 150 mM NaCl, and 1 mM β-mercaptoethanol under 40,000 rpm ultracentrifugation. The calculated molecular weights of each protein are listed in the figure. See also Supplement Data (Supplemental Fig. S1). (*E*) Endogenous Rrp46 either formed homodimers, or associated with a protein complex. Human (293T) and rice (callus) cell extracts were fractionated on a Superdex 200 gel-filtration column in a buffer with (+β-ME) or without β-mercaptoethanol and analyzed by Western blotting using rabbit anti-hRrp42, anti-hRrp46 or anti-oRrp46 serum. The hRrp42 was used as a control to show that it only associated with a protein complex. The cell extract before fractionation is shown in lane *L*.

Rice oRrp46 has DNase and RNase activity

The three Rrp46 proteins were incubated separately with DNA for gel retardation and DNA cleavage assays to determine their DNA-binding and cleavage activity (Fig. 3). The mobility of a ^{32}P-labeled 20-base-pair (bp) DNA was retarded by Rrp46/CRN-5, showing that the three recombinant proteins all bound to the double-stranded DNA (Fig. 3A). oRrp46 also degraded a linear 309-bp DNA, while hRrp46 and CRN-5 had no detectable DNase activity with a protein concentration of 1 μM in the time-course experiments (Fig. 3B), suggesting that the recombinant proteins hRrp46 and CRN-5 (and a negative control of RNase T) had either no or very low DNase activites in the in vitro condition. Divalent metal ions, preferably Ca^{2+} over Mg^{2+}, but not phosphate ions, were required for the DNase activity of oRrp46 (Fig. 3C), suggesting that oRrp46 was a hydrolase rather than a phosphorylase in the digestion of dsDNA. Moreover, oRrp46 cleaved the plasmid DNA, in contrast to an exonuclease TREX2, suggesting that oRrp46 has endonucleolytic DNase activity (Fig. 3D). Previously, the bacterial RNase PH has been shown to bind DNA (Jensen et al. 1992), and, for the first of time, we show here that an RNase PH family protein oRrp46 has metal-dependent hydrolytic DNase activity.

To determine the RNA-binding and cleavage activity, oRrp46, hRrp46, and CRN-5 were incubated with in vitro-transcribed 2.3-kb ssRNA for gel retardation and RNA cleavage assays. Figure 4, A and B, shows that oRrp46 had both RNA-binding and RNase activity against ssRNA. The retarded smears resulting from oRrp46 binding to the 2.3-kb RNA further suggest that multiple oRrp46 in high concentrations were bound to the large-size ssRNA, likely without sequence specificity, to induce the observable shifts. In contrast, CRN-5 and hRrp46 could not bind to or digest ssRNA.

To further confirm that oRrp46 is a phosphorylase, RNase assays were performed in the presence or absence of phosphate ions. oRrp46 digested a 20-nucleotide (nt) ssRNA only in the presence of both Mg^{2+} ions and

Downloaded from rnajournal.cshlp.org on April 26, 2024 - Published by Cold Spring Harbor Laboratory Press

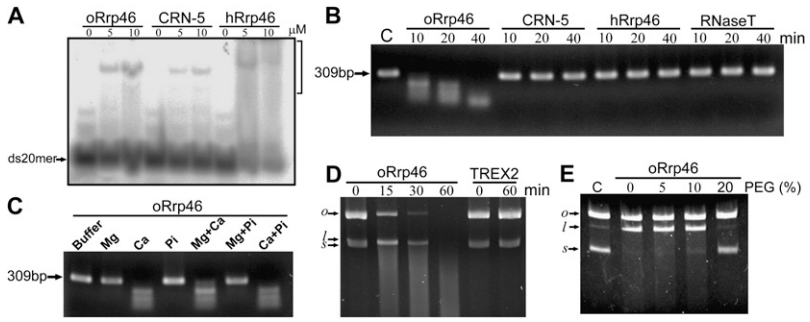

FIGURE 3. Rrp46 DNA-binding and DNase activity assays. (*A*) Gel-retardation assays show that Rrp46 binds to double-stranded DNA. Rrp46 (0, 5, and 10 μM) were incubated with 20-mer DNA (20 nM) in the buffer of 20 mM HEPES (pH 7.0) and 5 mM EDTA. The protein–DNA complexes were indicated by a bracket marked at the *right* of the panel. (*B*) DNA cleavage assays show that only rice oRrp46 cleaved double-stranded linear DNA. Rrp46 (1 μM) was incubated with the linear dsDNA (30 nM) in the DNase reaction buffer (20 mM HEPES [pH 7.0], 100 mM NaCl, 1 mM $CaCl_2$, and 1 mM DTT) at 37°C for the indicated periods, followed by agarose gel electrophoresis. A control reaction without any Rrp46 added is shown in lane *C*. RNA-specific RNase T was used as a negative control. (*C*) Rice oRrp46 is a metal ion-dependant hydrolytic DNase. oRrp46 (1 μM) was incubated with linear dsDNA (30 nM) at 37°C for 20 min in the presence or absence of $MgCl_2$, $CaCl_2$, and NaH_2PO_4. All the reaction buffers contained 20 mM HEPES (pH 7.0), 100 mM NaCl, and 1 mM DTT with addition of 2 mM $MgCl_2$ in lane *Mg*, 1 mM $CaCl_2$ in lane *Ca*, 5 mM NaH_2PO_4 in lane *Pi*, and combinations of each of two factors in the rest of the lanes. A control reaction without metal and phosphate ion added is shown in lane *Buffer*. (*D*) Rice oRrp46 cleaves plasmid DNA. oRrp46 (0.2 μM) was incubated with 100 ng plasmid DNA at 37°C for up to 60 min in the DNase reaction buffer. TREX2, an exonucleolytic hydrolase, was used as a negative control: *o*, open circular; *l*, linear; *s*, super coiled. (*E*) Rice oRrp46 lost its DNase activity in the presence of PEG3350. oRrp46 (0.2 μM) was incubated with 100 ng plasmid DNA at 37°C for 30 min in the presence of various concentration (0%–20%) of PEG3350. Lane *C* is for loading control: *o*, open circular; *l*, linear; *s*, super coiled.

phosphate ions (Fig. 4C). Moreover, using an in vitro-transcribed [α-^{32}P]ATP-incorporated single-stranded RNA as the substrate, oRrp46 cleaved ssRNA into ADP but not AMP (Fig. 4D), further confirming that oRrp46 was a phosphorolytic RNase. Altogether, these results suggest that rice oRrp46 is not only a hydrolytic DNase but also a phosphorolytic RNase, whereas the human hRrp46 and the worm homolog CRN-5 are only capable of binding to DNA but have neither DNase nor RNase activity.

Overall crystal structures of oRrp46 and CRN-5

To elucidate the molecular basis of oRrp46 and CRN-5 in domain assembly and nucleic acid cleavage activity, we crystallized the two proteins for three-dimensional structural determination. oRrp46 crystallized in the trigonal space group $P3_1$ with three molecules per asymmetric unit, diffracting X-rays to a resolution of 2.0 Å, whereas CRN-5 crystallized in the monoclinic space group $P2_1$ with two molecules per asymmetric unit, diffracting X-rays to a resolution of only 3.9 Å. Both structures were solved by molecular replacement using the crystal structure of human Rrp46 (PDB accession code 2NN6, chain D) as the search model. The statistics for X-ray diffraction and structural refinement are listed in Table 1.

oRrp46 was a dimer in solution; however, the three molecules in the asymmetric unit shared little contact area with buried interfaces <300 Å^2 for each subunit. To confirm the oligomeric state in the crystals, we found that oRrp46 was a monomer in the crystallization condition with a buffer solution containing 5% PEG3350 using gel filtration assays (see the elution profile marked with oRrp46/PEG in Fig. 2B). The human hRrp46 in the reconstituted six-subunit exosome complex also migrated as a monomer in the gel filtration analysis under low-salt conditions, suggesting that hRrp46 dimers may be dissociated into monomers at a low-ionic-strength condition (Liu et al. 2006). Moreover, we found that oRrp46 lost its DNase activity in the presence of 20% PEG3350, indicating that the dimeric conformation is important for the DNase activity (see Fig. 3E). Therefore oRrp46 was crystallized in a monomeric form, dissociated by PEG3350. The final model had an R-factor/R-free of 0.169/0.235 for 54,728/2776 reflections at a resolution of 2.0 Å.

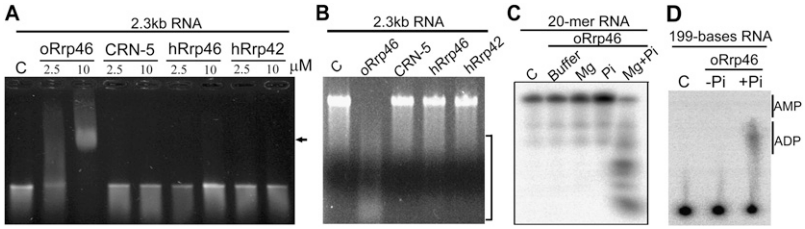

FIGURE 4. Rrp46 RNA-binding and RNase activity assays. (*A*) Gel retardation assays show that only rice oRrp46 binds to RNA. In vitro-transcribed RNA (500 ng) was incubated with Rrp46 (2.5 or 10 μM) in the RNA-binding buffer (50 mM Tris, pH 8.0, 10 mM EDTA, 1 U/μL RNaseIN) on ice for 30 min. The up-shifted RNA was indicated by an arrow. (*B*) RNA cleavage assays show that rice oRrp46 degrades RNA substrates. The bracket marked at the *right* indicates the degraded RNA. Rrp46 (5 μM) was incubated with the same substrate used in Figure 4A in the RNase reaction buffer (50 mM Tris [pH 8.0], 50 mM KCl, 2 mM $MgCl_2$, 5 mM Na_2HPO_4, and 1U/μL RNaseIN) at 30°C for 1 h followed by agarose gel electrophoresis. (*C*) Rice oRrp46 is a metal ion- and phosphate-dependent RNase. oRrp46 (2 μM) was incubated with 5′-labeled 20-mer ssRNA in conditions mentioned in Figure 3C. A control reaction with both cofactors but without any Rrp46 added is shown in lane *C*. (*D*) Thinlayer chromatography (TLC) separation of the final RNA reaction products cleaved by rice oRrp46. The internal ^{32}P-labeled RNA substrate was incubated with oRrp46 for 60 min with or without the presence of 5 mM phosphate (−Pi and +Pi). Positions of the cofractionated unlabeled ADP and AMP are shown on the *right*.

Downloaded from rnajournal.cshlp.org on April 26, 2024 - Published by Cold Spring Harbor Laboratory Press

TABLE 1. X-ray data collection and refinement statistics for rice oRrp46 and *C. elegans* CRN-5

Statistics	oRrp46	CRN-5
Data collection		
Space group	$P3_1$	$P2_1$
Cell dimensions (Å/degree)	a = 111.61 α = 90 b = 111.61 β = 90 c = 57.70 γ = 120	a = 61.92 α = 90 b = 44.83 β = 100.67 c = 65.58 γ = 90
Wavelength (Å)	1.00	1.00
Resolution (Å)	50.00–2.00 (2.07–2.00)[a]	50.00–3.90 (4.04–3.90)[a]
Observed reflections	185,470	9991
Unique reflections	55,506	3235
Completeness (%)	99.8 (99.7)	97.7 (91.3)
<I>/<σI>	21.65 (3.16)	14.06 (5.28)
R_{sym}[b](%)	6.50 (35.40)	9.1 (26.70)
Refinement		
Resolution range (Å)	50.00–2.00	50.00–3.90
Reflections (working/test)	54,782/2776	3217/227
R-factor/R-free (%)	16.9/23.5	30.7/35.6
Number of atoms (protein/water)	4687/416	2576/0
Average B-factor (Å^2)	26.1	87.9
RMS deviations (bond length [Å]/bond angle [degree])	0.006/1.090	0.005/0.989
Ramachandran plot (%)		
Most favored/additional allowed/generously allowed/disallowed	89.2/10.6/0.2/0.0	66.5/28.2/3.9/1.4

[a]Highest resolution shell is shown in parentheses.
[b]$R_{sym} = \Sigma hkl \Sigma i \mid Ii(hkl) - \langle I(hkl) \rangle \mid Ii(hkl)$.

The monomeric oRrp46 adopts a β-α-β-α folding and shares a similar structure to other RNase PH exonucleases (Fig. 5A). Superposition of oRrp46 onto hRrp46 by the secondary-structure-based method gave an RMSD of 1.29 Å over 187 C_α atoms. Superposition of oRrp46 onto archaeal Rrp41–Rrp42 dimer (PDB accession code: 2JEA) gave an RMSD of 1.32 Å over 202 C_α atoms against the active Rrp41, and 1.49 Å over 197 C_α atoms against the inactive Rrp42. This result suggests that oRrp46 shares a similar overall structure to other RNase PH family proteins with or without RNase activity.

To understand how Rrp46 monomers associate into a dimer, CRN-5 was crystallized in the conditions favoring homodimer formation. The resolution of the CRN-5 structure was only 3.9 Å, but this was sufficient to reveal the overall folding and dimeric assembly. The crystal structure of the dimeric CRN-5 is shown in Figure 5C, with a major interface contributed to by two antiparallel β-strands (residues 170–176) (see Fig. 1, β10). A hydrophobic area formed by the residues FIQL (180–183) of the α4 helix also stabilized the dimeric interface.

The CRN-5 structure is the first homodimeric structure observed in the RNase PH family proteins, the rest of which all crystallized in trimeric or hexameric forms with six RNase PH domains forming a ring-like structure, including the human exosome (Liu et al. 2006), the archaeal exosome (Buttner et al. 2005; Lorentzen and Conti 2005; Lorentzen et al. 2005; Navarro et al. 2008), bacterial PNPase (Symmons et al. 2000; Shi et al. 2008), and RNase PH (Ishii et al. 2003; Harlow et al. 2004). Superposition of the CRN-5 dimer over hRrp46-hRrp43 gave a RMSD of 3.05 Å over 273 C_α atoms, whereas superposition of the CRN-5 dimer onto the archaeal Rrp41–Rrp42 dimer (PDB accession code: 2JEA) gave a RMSD of 3.02 Å over 279 C_α atoms. These results suggest that the dimeric assembly mode of CRN-5 is similar to the one that exists between hRrp43 and hRrp46 in the human exosome, and to the one between Rrp41 and Rrp42 in archaeal exosomes.

Residues involved in substrate binding and cleavage in oRrp46

oRrp46 has both DNase and RNase activity, so the next question that arose was where the substrate-binding and active sites are in the dimeric oRrp46. The active residues of the phosphorolytic RNase PH domain have been well studied in archaeal exosomes (Buttner et al. 2005; Lorentzen and Conti 2005; Navarro et al. 2008). One acidic residue (D182 in *Sulfolobus sulfataricus*, D180 in *Pyrococcus abyssi*) is critical for the RNase activity of archaeal Rrp41, and this acidic residue is conserved in both active and inactive RNase PH proteins, including D486 of PNPase, E174 of hRrp46, E219 of hRrp42, D180 of PaRrp41, and E160 of oRrp46. The recent crystal structure analysis of the *E. coli* PNPase bound to manganese further suggests that this conserved acidic residue (D486) is bound to the metal ion, responsible for stabilizing the transition state (Nurmohamed et al. 2009). Superposition of the structure of oRrp46 with all of these RNase PH enzymes showed that E160 in oRrp46 fitted well with the conserved acidic residues (marked by an arrow in Fig. 5A). We therefore mutated E160 to determine whether this residue is a catalytic residue in oRrp46. As a result, the purified oRrp46 E160Q lost most of its DNase activity in digesting a linear 309-bp dsDNA (see Fig. 6A); however, the mutant only lost partial activity in digesting a 20-mer ssRNA (Fig. 6B). These results suggest that E160 plays a more important role in catalyzing the hydrolytic cleavage of DNA, and it plays a less critical role in the phosphorolytic cleavage of RNA.

To determine the residues involved in nucleic acid binding, we compared the crystal structures of oRrp46 with those of active archaeal Rrp41 (PDB accession code: 2PO1, chain B) and human hRrp46 (PDB accession code: 2NN6, chain D). A 5-nt RNA substrate bound in the

Downloaded from rnajournal.cshlp.org on April 26, 2024 - Published by Cold Spring Harbor Laboratory Press

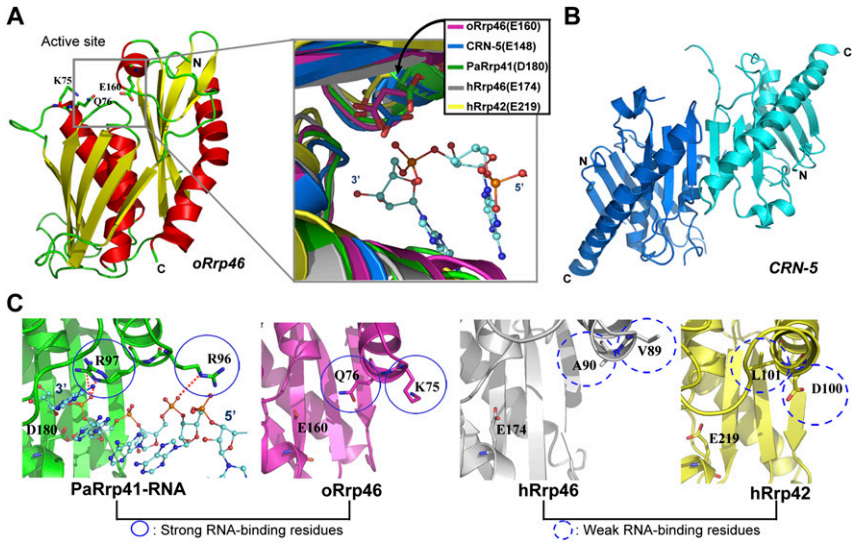

FIGURE 5. Crystal structures of the monomeric oRrp46 and dimeric CRN-5. (*A*) The crystal structure of the monomeric oRrp46. The catalytic residue, E160, and substrate-binding residues, K75 and Q76, in the active site are shown as a stick model. (*B*) Superposition of the active sites of several RNase PH proteins shows that a conserved acidic residue is located at the same position: E160 in oRrp46 (this study), E148 in CRN-5 (this study), D180 in PaRrp42 (2PO1, chain A), E174 in hRrp46 (2NN6, chain D), and E219 in hRrp42 (2NN6, chain E). The bound RNA nucleotide cocrystallized with PaRrp41 is displayed as a ball-and-stick model. (*C*) The crystal structure of the dimeric CRN-5. Individual monomers are shown in blue and cyan, respectively. Comparison of RNA-binding residues in RNase PH proteins. The two basic residues, R96 and R97, bind to the phosphate groups of RNA (displayed as a ball-and-stick model) in PaRrp41 (green, 2PO1, chain A). Corresponding residues in oRrp46 (Q76 and K75) are more suitable for RNA binding compared with those in the inactive enzymes of hRrp46 (V89 and A90) and hRrp42 (D100 and L101). The strong RNA-binding residues are circled in solid lines and the weak RNA-binding residues are circled in dashed lines.

structure of the *P. abyssi* Rrp41–RNA complex reveals two important basic residues, R96 and R97, involved in RNA binding (circled in Fig. 5C; Navarro et al. 2008). These two basic residues are missing in the inactive hRrp46 (Fig. 5C, gray, V89 and A90) and hRrp42 (Fig. 5C, yellow, D100 and L101), suggesting that the loss of RNase activity is likely a result of the loss of RNA-binding activity. In oRrp46 a polar (Q76) and a basic (K75) residue are located at the corresponding RNA-binding site and may play a similarly important role in RNA binding. To verify our hypothesis, we constructed a double mutant of oRrp46, K75E/Q76E, to test its RNA-binding and cleavage activity. This oRrp46 mutant (K75E/Q76E) almost completely lost its DNA- and RNA-binding activity in gel retardation assays (Fig. 6C,D). The DNase and RNase activity were also abolished, compared with the wild-type oRrp46 (Fig. 6A,B). Therefore, K75 and Q76 of oRrp46 are indeed involved in RNA and DNA binding. Impairment of the substrate-binding ability of oRrp46 results in the loss of its nuclease activity.

CRN-5 interacts with CRN-4 and enhances the DNase activity of CRN-4

CRN-5 was identified as a cell death-related nuclease involved in DNA fragmentation during apoptosis in *C. elegans* (Parrish and Xue 2003). However, here we show that CRN-5 only binds to DNA without detectable DNase activity. It was therefore puzzling how CRN-5 is involved in DNA fragmentation. It has been shown previously that CRN-5 is a component of a protein complex, the degradeosome, interacting with CPS-6, CRN-4, CRN-1, and CYP-13 in GST pull-down assays (Parrish and Xue 2003). To further clarify the role of CRN-5 in DNA degradation, we tested its interaction with CRN-4, a fully characterized DEDD family apoptotic nuclease with both DNase and RNase activity (Hsiao et al. 2009). We confirmed that His-tagged dimeric CRN-5 interacted directly with dimeric CRN-4 by His-tag pull-down assays (see Fig. 7A; Parrish and Xue 2003). Moreover, the DNase activity of CRN-4 was enhanced by the presence of CRN-5 compared with that of CRN-4 alone (Fig. 7B, cf. 6.5% DNA remaining and 13% DNA remaining with CRN-4 alone). These results suggest that CRN-5 promotes CRN-4's DNase

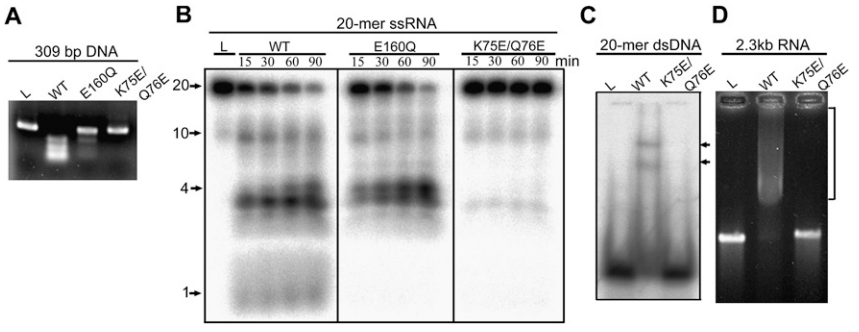

FIGURE 6. In vitro nuclease activity assays of wild-type and mutated oRrp46. (*A*) DNA (309 bp, 30 nM) cleavage assays by the wild type, active-site mutant (E160Q), and nucleotide-binding-site mutant (K75E/Q76E) of oRrp46 (1 μM). All the reaction conditions were identical to those in Figures 3 and 4. (*B*) Time-course RNA cleavage assays by the wild type, E160Q, and K75E/Q76E mutant of oRrp46. The RNA markers that varied from 1 to 20 nucleotide(*s*) are labeled on the *left* of the panel. (*C*) DNA gel shift assays of the wild type and K75E/Q76E mutant of oRrp46. The protein–DNA complex is indicated with an arrow. (*D*) RNA gel shift assays of the wild type and K75E/Q76E mutant of oRrp46. The up-shifted RNA is indicated by arrows. The bracket at the *right* indicates the up-shifted RNA.

Downloaded from rnajournal.cshlp.org on April 26, 2024 - Published by Cold Spring Harbor Laboratory Press

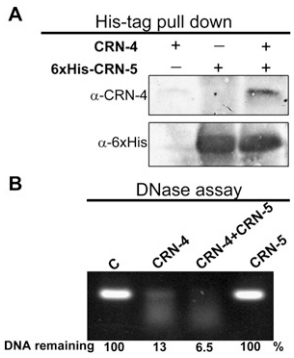

FIGURE 7. CRN-5 interacts with CRN-4 and enhances CRN-4's DNase activity. (*A*) His-tag pull-down assays of CRN-4 by His-tagged CRN-5. The His-tagged CRN-5 was incubated with or without CRN-4, and then the complex was pulled down in a Ni-NTA spin column. The eluted solution was analyzed by Western blotting using anti-CRN-4 (α-CRN-4) and anti-6xHis (α-6xHIS) antibodies. (*B*) Assays of CRN-4 DNase activity in the presence or absence of CRN-5. A linear 309-bp double-stranded DNA (30 nM) was incubated with CRN-4 (1 μM), CRN-5 (2 μM), or both together, and the DNA digests were analyzed and quantified by gel electrophoresis. CRN-4 cleaved linear dsDNA more efficiently in the presence of inactive CRN-5 (6.5% vs. 13% DNA remained).

activity and these two proteins act cooperatively in DNA degradation.

DISCUSSION

RNA-binding residues are critical for the enzyme activity of RNase PH proteins

RNase PH family proteins are a group of fascinating enzymes, sharing similar sequences and structures, but they have evolved differently with either retained or lost RNase activity (Symmons et al. 2002). They can be grouped into active RNases, which include RNase PH, the second PH domain of PNPase, archaeal Rrp41, plant Rrp41 and oRrp46, and inactive RNases, including the first PH domain of PNPase, archaeal Rrp42, and all the human and yeast RNase PH proteins in exosomes. The structural basis of an active versus an inactive RNase PH enzyme in RNA cleavage is still under discussion. Previous studies have focused on the comparison of the conserved general-acid residue and the varied phosphate-binding residues among the RNase PH family proteins (Buttner et al. 2005; Lorentzen and Conti 2005; Navarro et al. 2008).

Here we identify a quite significant feature in RNase PH family proteins that differentiates an active enzyme from an inactive one. We found that the active oRrp46 has a positively charged region located at the RNA entry site (due to "strong RNA-binding residues," shown in Fig. 5C), which may facilitate RNA binding (marked by a red circle in Fig. 8). A similar positively charged RNA-binding region can be observed on the active enzymes of archaeal Rrp41 (PaRrp41) and the second domain of PNPase (PNPase_RNase PH II). On the contrary, the surface of the corresponding regions on the inactive enzymes, including archaeal Rrp42 (PaRrp42), the first domain of PNPase (PNPase_RNase PH I) and human Rrp46, are neutral or even acidic, and thus not suitable for RNA binding (marked by a green circle in Fig. 8). The loss of nucleic acid-binding ability in the oRrp46 K75E/Q76E mutant resulted in the loss of its RNA cleavage activity, further supporting this suggestion that the ability to bind substrates is closely related to the nuclease activity of an RNase PH enzyme. This observation is true for all the RNase PH proteins with known structures, except for the inactive human Rrp41, which has suitable residues for the role of general acid and phosphate binding, and also appropriate residues for RNA binding (Lorentzen and Conti 2005). Therefore, we conclude that possessing the correct RNA-binding residues at the entry site of an RNase PH protein is a necessary, but not sufficient, condition for efficient RNase activity.

Dual roles of Rrp46 in RNA turnover and DNA degradation

Our biochemical and structural analyses demonstrate that the eukaryotic exosomal component proteins, including hRrp46 and oRrp46, form a stable homodimer in vivo and in vitro. The homodimeric rice oRrp46 shows, for the first time, both hydrolytic DNase and phosphorolytic RNase activity. On the other hand, the nematode Rrp46 (CRN-5) and human hRrp46 had no detectable DNase and RNase activities. It has been shown that Rrp41 from *Arabidopsis*

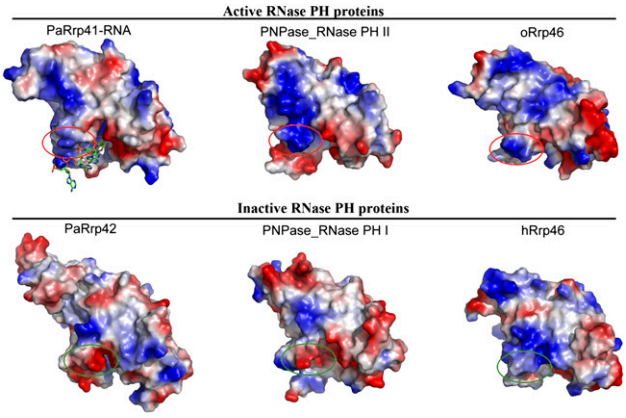

FIGURE 8. Electrostatic surface potential and substrate-binding sites of active and inactive RNase PH proteins. The active RNase PH proteins all have positive surfaces at the RNA-binding site (circled), including PaRrp41 (2PO1, chain A), RNase PH II domain of PNPase (3CDI), and oRrp46 (this study). The RNA bound in PaRrp41 is displayed as a stick model. On the contrary, the inactive RNase PH proteins have neutral or acidic surfaces at the RNA-binding sites (circled), including PaRp42 (2PO1, chain B), RNase PH I domain of PNPase (3CDI), and hRrp46. The color scale of the surface potential was set from −75 kT/e (red) to 75 kT/e (blue), as calculated by Pymol (DeLano Scientific LLC, http://www.pymol.org).

Downloaded from rnajournal.cshlp.org on April 26, 2024 - Published by Cold Spring Harbor Laboratory Press

thaliana displays a processive phosphorolytic exoribonuclease activity (Chekanova et al. 2000). Our results show, without forming an exosome complex, that homodimeric oRrp46 alone is also an active phosphorolytic RNase. The RNase activity of oRrp46 can be abolished by substrate-binding site (K75 and Q76) mutation, excluding the possibility of contamination by *E. coli* enzymes during protein preparation. This result thus shows that eukaryotic exosome core complexes have evolved distinctive ways of degrading RNA, as some of the plant exosome RNase PH component proteins do have RNase activities, compared with the yeast and human exosomal proteins which have no detectable activity.

Rrp46/CRN-5 is also a candidate for apoptotic DNA degradation in *C. elegans* (Parrish and Xue 2003). Here we show that rice oRrp46 indeed has DNase activity, and *C. elegans* CRN-5 enhances the DNase activity of CRN-4. These results provide new lines of evidence to support the involvement of Rrp46 in apoptotic nucleosomal degradation. Although CRN-5 only increases the DNase activity of CRN-4 slightly in vitro, it is likely that various apoptotic nucleases in the degradeosome complex, including CPS-6, CRN-1, CRN-3, CRN-4, CRN-5, and CYP-13, work together and increase the efficiency of DNA degradation with a synergistic effect in cellular environments. Another exosome component protein, CRN-3, a homolog of human PM-Scl100 and yeast Rrp6, is also implicated in the degradeosome and is suggested to be involved in DNA degradation during apoptosis (Parrish and Xue 2003). Therefore, CRN-5 is not the only exosome component protein that is identified as a player in DNA fragmentation during apoptosis.

Interestingly, autoantibodies against both PM-Scl100 and hRrp46 are often identified in the patients with autoimmune diseases (Reichlin et al. 1984; Bluthner and Bautz 1992; Ge et al. 1992; Brouwer et al. 2002). Loss or reduction of DNase activity of several nucleases has been shown to link to a number of autoimmune diseases, such as DNase I associated with systemic lupus erythmatosus (Napirei et al. 2000; Yasutomo et al. 2001), and DNase II associated with rheumatoid arthritis (Kawane et al. 2006). It is suggested that the DNA escaping from degradation during program cell death elicits autoimmune responses; however, the underlying mechanisms and signaling events that regulate innate immune responses to extracellular and cytosolic undigested DNA are still elusive (Green et al. 2009; Okabe et al. 2009). The finding of autoantibodies of hRrp46 and PM-Scl100 in autoimmune diseases hints at a link between the two exosome component proteins and DNA degradation.

A search in the cancer database further shows that hRrp46 is up-regulated in various cancer tissues, including eye, lung, placenta, and skin cancers (Krizman et al. 1999). This up-regulation trend is, however, not observed for other exosomal RNase PH proteins, further suggesting that hRrp46 may play a function other than RNA turnover and processing. In summary, our results strongly support the notion that Rrp46/CRN-5 forms a homodimer, participating in DNA degradation in cell death. Rrp46 likely switches its role and plays dual functions between life and death. Based on these biochemical, cellular, structural. and mutational results, we suggest that Rrp46 is not only an exosome component protein participating in RNA degradation and processing, but that it also forms a homodimer involved in DNA degradation in apoptosis. This finding therefore opens a new direction for the future study of hRrp46 to uncover its link to autoimmune diseases and cancer.

MATERIALS AND METHODS

Cloning, protein expression, and purification

Full-length cDNAs of human and of rice Rrp46 were purchased from OpenBiosystems (Clone ID: 4308795) and the KOME database (Clone ID: 204796), respectively. The genes of the full-length rice Rrp46 (oRrp46), CRN-5, and human Rrp46 (hRrp46) were PCR-amplified and cloned into expression vectors, pET-22b (Novagen), pQE-70 (Qiagen), and pET-28c (Novagen), respectively, to generate His-tagged fusion constructs. pQE-70-CRN5 expression plasmid was transformed into the *E. coli* M15 strain cultured in LB medium, supplemented with 100 μg/mL ampicillin. pET-22b-oRrp46 and pET-28c-hRrp46 were transformed into the *E. coli* BL21-CodonPlus(DE3)-RIPL strain (Stratagene) cultured with 75 μg/mL streptomycin, 50 μg/mL chloramphenicol, and 100 μg/mL ampicillin or 50 μg/mL kanamycin. The transformed bacterial expression strains were grown to an OD_{600} of 0.4 and then induced with 0.5 mM IPTG at 18°C for 20 h. The harvested cells were disrupted by a microfluidizer in the buffer of 50 mM Tris-HCl (pH 7.6), 300 mM NaCl, and 1 mM β-mercaptoethanol.

The crude cell extract was passed through a TALON metal affinity resin column (BD Biosciences) followed by a gel filtration chromatography column (Superdex 200; GE Healthcare). Purified protein samples were concentrated to a suitable concentration in 25 mM Tris-HCl (pH 7.6), 150 mM NaCl, and 1 mM β-mercaptoethanol. The homogeneity of the protein was analyzed by electrophoresis. Protein samples (2 μg) were mixed with the sample loading buffer containing the reducing agent (6 mM β-mercaptoethanol) and were heated to denature the protein before resolving the sample in 10% SDS-PAGE stained with Commassie blue (see Fig. 2A). All oRrp46 point mutants were generated by Quickchange site-directed mutagenesis kits (Stratagene) and purified by the same procedure as the wild-type oRrp46.

Dynamics light scattering and analytical ultracentrifugation

Dynamics light scattering (DLS) measurements were carried out on a Dyna-Pro 99 MS800 instrument (Protein Solutions). The purified protein (0.5 mg/mL) in a buffer of 20 mM HEPES (pH 7.0), 100 mM NaCl, 1 mM $CaCl_2$, and 1 mM DTT was centrifuged at 16,000*g*, 4°C for 15 min, and the supernatant was placed in a 12-μL cuvette (b = 1.5 mm). The protein samples were incubated

Downloaded from rnajournal.cshlp.org on April 26, 2024 - Published by Cold Spring Harbor Laboratory Press

for 5 min at 20°C before data acquisition over an acquired time of 15 min. The size distribution plots—the *x*-axis showing a distribution of estimated particle radius (nm) and the *y*-axis showing the relative intensity of the scattered light (percentage of intensity)—were analyzed with software Dynamics V5.26.60 (Protein Solutions).

For analytical ultracentrifugation (AUC) assays, the recombinant human hRrp46 and *C. elegans* CRN-5 were concentrated to an OD_{280} of 0.5 in 25 mM Tris-HCl (pH 7.6), 150 mM NaCl, and 1 mM β-mercaptoethanol. Sedimentation velocities of proteins were performed at 40,000 rpm (Beckman XL-A) under 4°C. Multiple scans (OD_{280}) at different time intervals were then fitted to a continuous c(s) distribution model using the SEDFIT program (Schuck 2000; Brown and Schuck 2006).

Fractionation of cell extracts and Western blotting

Human kidney 293T cells were pooled and extracted by sonication in 2 mL of PBS buffer (10 mM Na_2HPO_4, 1.8 mM KH_2PO_4, pH 7.4, 140 mM NaCl, and 2.7 mM KCl) with or without 1 mM β-mercaptoethanol. Rice callus cells were dried and extracted by grinding in liquid nitrogen and then dissolved in 2 mL PBS buffer. Crude cell extract was then centrifuged at 16,000*g*, 4°C for 15 min. The supernatant was collected and passed through a gel filtration chromatography column (Superdex 200, GE Healthcare). Eluted fractions were collected and concentrated using Vivaspin 6 centrifugal concentrators (GE Healthcare). Equal volumes of concentrated fractions were separated by SDS-PAGE, and probed by Western blotting using anti-hRrp46, anti-oRrp46, and anti-hRrp42 antibodies.

DNA-binding and DNase activity assays

For DNA gel shift assays, 20 nM of 5′-end P^{32}-labeled 20-nt double-stranded DNA (5′-ACTGGACAAATACTCCGAGG-3′) were incubated with different concentrations of purified recombinant protein in a buffer containing 20 mM HEPES (pH 7.0) and 5 mM EDTA on ice for 1 h After incubation, the reaction mixtures were resolved in 10% polyacrylamide gels, which were exposed to the phosphorimaging plate (Fujifilm) and analyzed by an FLA-5000 (Fujifilm) imaging system (Figs. 3A, 6C).

For the DNase activity assays shown in Figures 3, B and C, and 6A, 309-bp linear double-stranded DNA (30 nM) were incubated with the purified protein (1 μM) in the DNase reaction buffer containing 20 mM HEPES (pH 7.0), 100 mM NaCl, 1 mM $CaCl_2$, and 1 mM DTT at 37°C for the indicated periods. For the DNase activity assays shown in Figure 3D, a pQE-70 plasmid DNA (100 ng) was incubated with 0.2 μM purified protein in the DNase reaction buffer at 37°C for the indicated periods. For the DNase activity assays shown in Figure 7B, purified CRN-4 and/or CRN-5 (concentration 1–2 μM) was incubated with 309-bp double-stranded DNA (30 nM) in a solution of 10 mM NaCl, 3 mM $MgCl_2$, 1 mM $CaCl_2$, and 20 mM Tris-HCl (pH 6.0) at 30°C for 40 min. All the reactions were stopped by adding 10 mM proteinase K for 10 min to remove proteins. The digest patterns were resolved on 1% or 1.5% agarose gels stained by ethidium bromide and quantified by AlphaEaseFC software (Alpha Innotech).

RNA-binding and RNase activity assays

The 2.3-kb ssRNA was transcribed in vitro using a MAXIscript kit (Ambion). The 20-mer ssRNA (5′-ACUGGACAAAUACUCCGAGG-3′) was first labeled at the 5′ end with [γ-^{32}P] ATP by T4 polynucleotide kinase and then purified on a Microspin G-25 column (GE Healthcare) to remove the unincorporated nucleotides. For RNA-binding assays, 500 ng of 2.3-kb ssRNA substrates were incubated with different concentrations of recombinant purified protein in the RNA-binding buffer (50 mM Tris-HCl at pH 8.0, and 10 mM EDTA) on ice for 30 min. After incubation, the reaction mixture was separated on 1% agarose gels and stained with ethidium bromide.

For RNase activity assays, 20 nM of labeled 20-mer ssRNA or 500 ng 2.3-kb ssRNA substrates was incubated with different concentrations of purified protein in the RNase reaction buffer (50 mM Tris-HCl at pH 8.0, 50 mM KCl, 2 mM $MgCl_2$, 5 mM NaH_2PO_4, and RNase IN [1 U/μL, Promega]) at 30°C for 1 h. The reaction was stopped at the time point indicated in the figures by adding TBE-Urea sample buffer (Bio-Rad) or 10 mM proteinase K. Digest patterns of 20-mer ssRNA were resolved in 20% polyacrylamide/7 M urea gels, which were exposed to the phosphorimaging plate (Fujifilm) and analyzed by an FLA-5000 (Fujifilm) imaging system.

The RNA substrate used in the thin layer chromatography (Fig. 4D) was transcribed by T7 RNA polymerase with linearized (XhoI) pET-22b (Novagen) in the presence of [α-^{32}P]ATP. Ascending thin layer chromatography was done on polyethyleneimine-cellulose plates (Sigma) in 1.2 M formic acid and 0.5 M LiCl. The cold AMP and ADP standards (100 nmol) were added to the samples before loading. Standards were visualized by UV shadowing.

Crystallization and X-ray diffraction data collection

Crystals of CRN-5 and oRrp46 were grown by the hanging-drop vapor diffusion method at room temperature. The crystallization drop was made by mixing 1 μL of protein solution and 1 μL of reservoir solution. oRrp46 (7.5 mg/mL, 50 mM Tris-HCl, pH 8.0, 150 mM NaCl) was crystallized using a reservoir solution containing 0.2 M sodium malonate (pH 7.0) and 20% PEG3350. CRN-5 (30 mg/mL, 50 mM Tris-HCl at pH 8.0) was crystallized using a reservoir solution containing 0.1 M Tris-HCl (pH 8.0), 0.2 M NaCl, and 25% PEG3350. Diffraction data of oRrp46 and CRN-5 were collected at −150°C at beamlines 13C1 and 13B1, respectively, of the National Synchrotron Radiation Research Center, Taiwan, and were processed and scaled by HKL2000 (Otwinowski and Minor 1997). All diffraction statistics are listed in Table 1.

Structure determination and refinement

oRrp46 crystallized in the trigonal space group $P3_1$ as twin crystals with a twin factor of 0.5. The twin operation of the Miller index was assigned as (h,-h-k,-l) using Phenix (Xtriage) (Adams et al. 2002), as well as Merohedral Crystal Twinning Server (Yeates 1997). CRN-5 crystallized in the monoclinic space group $P2_1$ with two molecules per asymmetric unit. The structure oRrp46 and CRN-5 were solved by molecular replacement by CCP4-Molrep (Potterton et al. 2003) and BALBES (Long et al. 2008), respectively, using the crystal structure of human Rrp46 (PDB accession code: 2NN6, chain D) as the search model. The protein model was constructed using the program Coot (Emsley and Cowtan 2004) and refined by Phenix (Adams et al. 2002). Due to the low resolution of the CRN-5 data (3217 unique reflections),

Downloaded from rnajournal.cshlp.org on April 26, 2024 - Published by Cold Spring Harbor Laboratory Press

the CRN-5 structure was refined in the final stage by rigid-body refinements followed by group B factor refinements (one residue per group). The stereochemical quality of the refined model was evaluated by PROCHECK (Laskowski et al. 1993). Structural coordinates and diffraction structure factors have been deposited in the RCSB Protein Data Bank with the PDB ID code of 3HKM for oRrp46 and 3KRN for CRN-5.

His-tag pull-down assays

His-tagged CRN-5 (5 μg) was incubated with CRN-4 (5 μg) in 50 mM Tris-HCl, 300 mM NaCl at pH 7.5, at 4°C for 8 h. After centrifugation, the protein sample was loaded onto Ni-NTA spin columns (Qiagen) and washed three times each with Wash-1 buffer and Wash-2 buffer (Wash-1 buffer: 50 mM Tris-HCl, 300 mM NaCl [pH 7.5], and 2 mM imidazole; Wash-2 buffer: 50 mM Tris-HCl, 300 mM NaCl [pH 7.5], and 5 mM imidazole). Bound proteins eluted with elution buffer (50 mM Tris-HCl, 300 mM NaCl [pH 7.5], and 500 mM imidazole) were separated by SDS-PAGE in 10% gels. CRN-4 and His-tagged CRN-5 were probed with anti-CRN-4 and anti-His tag antibodies (Novagen) after transferring onto a PVDF membrane. Detection was carried out using alkaline phosphatase-conjugated secondary antibody (Millipore) and BCIP/NBT substrate solution.

SUPPLEMENTAL DATA

Supplemental material can be found at http://www.rnajournal.org.

ACKNOWLEDGMENTS

This work was supported by research grants from Academia Sinica and the National Science Council, Taiwan. Portions of this research were carried out at the National Synchrotron Radiation Research Center (BL-13B1 and BL-13C1), a national user facility supported by the National Science Council of Taiwan. The Synchrotron Radiation Protein Crystallography Facility is supported by the National Research Program for Genomic Medicine. We thank Ding Xue at the University of Colorado for providing the cDNA of CRN-4 and CRN-5. We also thank Su-May Yu at Academia Sinica for providing the rice callus for protein analysis, and Ethan Wu at Biophysics Core Facility, Academia Sinica, for AUC data collection.

Received March 17, 2010; accepted June 10, 2010.

REFERENCES

Adams PD, Grosse-Kunstleve RW, Hung LW, Ioerger TR, McCoy AJ, Moriarty NW, Read RJ, Sacchettini JC, Sauter NK, Terwilliger TC. 2002. PHENIX: Building new software for automated crystallographic structure determination. *Acta Crystallogr D Biol Crystallogr* **58:** 1948–1954.

Allmang C, Kufel J, Chanfreau G, Mitchell P, Petfalski E, Tollervey D. 1999a. Functions of the exosome in rRNA, snoRNA, and snRNA synthesis. *EMBO J* **18:** 5399–5410.

Allmang C, Petfalski E, Podtelejnikov A, Mann M, Tollervey D, Mitchell P. 1999b. The yeast exosome and human PM-Scl are related complexes of 3′ → 5′ exonucleases. *Genes Dev* **13:** 2148–2158.

Anderson JS, Parker RP. 1998. The 3′ to 5′ degradation of yeast mRNAs is a general mechanism for mRNA turnover that requires the SKI2 DEVH box protein and 3′ to 5′ exonucleases of the exosome complex. *EMBO J* **17:** 1497–1506.

Andrulis ED, Werner J, Nazarian A, Erdjument-Bromage H, Tempst P, Lis JT. 2002. The RNA processing exosome is linked to elongating RNA polymerase II in Drosophila. *Nature* **420:** 837–841.

Bluthner M, Bautz FA. 1992. Cloning and characterization of the cDNA coding for a polymyositis–scleroderma overlap syndrome-related nucleolar 100-kD protein. *J Exp Med* **176:** 973–980.

Bonneau F, Basquin J, Ebert J, Lorentzen E, Conti E. 2009. The yeast exosome functions as a macromolecular cage to channel RNA substrates for degradation. *Cell* **139:** 547–559.

Brouwer R, Vree Egberts WT, Hengstman GJ, Raijmakers R, van Engelen BG, Seelig HP, Renz M, Mierau R, Genth E, Pruijn GJ, et al. 2002. Autoantibodies directed to novel components of the PM/Scl complex, the human exosome. *Arthritis Res* **4:** 134–138.

Brown PH, Schuck P. 2006. Macromolecular size-and-shape distributions by sedimentation velocity analytical ultracentrifugation. *Biophys J* **90:** 4651–4661.

Buttner K, Wenig K, Hopfner KP. 2005. Structural framework for the mechanism of archaeal exosomes in RNA processing. *Mol Cell* **20:** 461–471.

Chekanova JA, Shaw RJ, Wills MA, Belostotsky DA. 2000. Poly(A) tail-dependent exonuclease AtRrp41p from *Arabidopsis thaliana* rescues 5.8 S rRNA processing and mRNA decay defects of the yeast ski6 mutant and is found in an exosome-sized complex in plant and yeast cells. *J Biol Chem* **275:** 33158–33166.

de la Cruz J, Kressler D, Tollervey D, Linder P. 1998. Dob1p (Mtr4p) is a putative ATP-dependent RNA helicase required for the 3′ end formation of 5.8S rRNA in *Saccharomyces cerevisiae*. *EMBO J* **17:** 1128–1140.

Deutscher MP, Marshall GT, Cudny H. 1988. RNase PH: An *Escherichia coli* phosphate-dependent nuclease distinct from polynucleotide phosphorylase. *Proc Natl Acad Sci* **85:** 4710–4714.

Dziembowski A, Lorentzen E, Conti E, Seraphin B. 2007. A single subunit, Dis3, is essentially responsible for yeast exosome core activity. *Nat Struct Mol Biol* **14:** 15–22.

Emsley P, Cowtan K. 2004. Coot: Model-building tools for molecular graphics. *Acta Crystallogr D Biol Crystallogr* **60:** 2126–2132.

Estevez AM, Kempf T, Clayton C. 2001. The exosome of *Trypanosoma brucei*. *EMBO J* **20:** 3831–3839.

Evguenieva-Hackenberg E, Walter P, Hochleitner E, Lottspeich F, Klug G. 2003. An exosome-like complex in *Sulfolobus solfataricus*. *EMBO Rep* **4:** 889–893.

Ge Q, Frank MB, O'Brien C, Targoff IN. 1992. Cloning of a complementary DNA coding for the 100-kD antigenic protein of the PM-Scl autoantigen. *J Clin Invest* **90:** 559–570.

Gouet P, Robert X, Courcelle E. 2003. ESPript/ENDscript: Extracting and rendering sequence and 3D information from atomic structures of proteins. *Nucleic Acids Res* **31:** 3320–3323.

Green DR, Ferguson T, Zitvogel L, Kroemer G. 2009. Immunogenic and tolerogenic cell death. *Nat Rev Immunol* **9:** 353–363.

Harlow LS, Kadziola A, Jensen KF, Larsen S. 2004. Crystal structure of the phosphorolytic exoribonuclease RNase PH from *Bacillus subtilis* and implications for its quaternary structure and tRNA binding. *Protein Sci* **13:** 668–677.

Hilleren P, McCarthy T, Rosbash M, Parker R, Jensen TH. 2001. Quality control of mRNA 3′-end processing is linked to the nuclear exosome. *Nature* **413:** 538–542.

Hsiao YY, Nakagawa A, Shi Z, Mitani S, Xue D, Yuan HS. 2009. Crystal structure of CRN-4: Implications for domain function in apoptotic DNA degradation. *Mol Cell Biol* **29:** 448–457.

Ishii R, Nureki O, Yokoyama S. 2003. Crystal structure of the tRNA processing enzyme RNase PH from *Aquifex aeolicus*. *J Biol Chem* **278:** 32397–32404.

Jensen KF, Andersen JT, Poulsen P. 1992. Overexpression and rapid purification of the orfE/rph gene product, RNase PH of *Escherichia coli*. *J Biol Chem* **267:** 17147–17152.

Downloaded from rnajournal.cshlp.org on April 26, 2024 - Published by Cold Spring Harbor Laboratory Press

Kadaba S, Krueger A, Trice T, Krecic AM, Hinnebusch AG, Anderson J. 2004. Nuclear surveillance and degradation of hypomodified initiator tRNAMet in *S. cerevisiae*. *Genes Dev* **18:** 1227–1240.

Kawane K, Ohtani M, Miwa K, Kizawa T, Kanbara Y, Yoshioka Y, Yoshikawa H, Nagata S. 2006. Chronic polyarthritis caused by mammalian DNA that escapes from degradation in macrophages. *Nature* **443:** 998–1002.

Koonin EV, Wolf YI, Aravind L. 2001. Prediction of the archaeal exosome and its connections with the proteasome and the translation and transcription machineries by a comparative-genomic approach. *Genome Res* **11:** 240–252.

Krizman DB, Wagner L, Lash A, Strausberg RL, Emmert-Buck MR. 1999. The Cancer Genome Anatomy Project: EST sequencing and the genetics of cancer progression. *Neoplasia* **1:** 101–106.

Laskowski RA, MacArthur MW, Moss DS, Thornton JM. 1993. PROCHECK: A program to check the stereochemical quality of protein structures. *J Appl Crystallogr* **26:** 283–291.

Littauer UZ, Grunberg-Manago M. 1999. Polynucleotide phosphorylase. In *The encyclopedia of molecular biology*, (ed. TE Creighton). pp. 1911–1918. Wiley, New York.

Liu Q, Greimann JC, Lima CD. 2006. Reconstitution, activities, and structure of the eukaryotic RNA exosome. *Cell* **127:** 1223–1237.

Long F, Vagin AA, Young P, Murshudov GN. 2008. BALBES: A molecular-replacement pipeline. *Acta Crystallogr D Biol Crystallogr* **64:** 125–132.

Lorentzen E, Conti E. 2005. Structural basis of 3′ end RNA recognition and exoribonucleolytic cleavage by an exosome RNase PH core. *Mol Cell* **20:** 473–481.

Lorentzen E, Walter P, Fribourg S, Evguenieva-Hackenberg E, Klug G, Conti E. 2005. The archaeal exosome core is a hexameric ring structure with three catalytic subunits. *Nat Struct Mol Biol* **12:** 575–581.

Mitchell P, Tollervey D. 2003. An NMD pathway in yeast involving accelerated deadenylation and exosome-mediated 3′→5′ degradation. *Mol Cell* **11:** 1405–1413.

Mitchell P, Petfalski E, Shevchenko A, Mann M, Tollervey D. 1997. The exosome: A conserved eukaryotic RNA processing complex containing multiple 3′→5′ exoribonucleases. *Cell* **91:** 457–466.

Napirei M, Karsunky H, Zevnik B, Stephan H, Mannherz HG, Moroy T. 2000. Features of systemic lupus erythematosus in DNase I deficient mice. *Nat Genet* **25:** 177–181.

Navarro MV, Oliveira CC, Zanchin NI, Guimaraes BG. 2008. Insights into the mechanism of progressive RNA degradation by the archaeal exosome. *J Biol Chem* **283:** 14120–14131.

Nurmohamed S, Vaidialingam B, Callaghan AJ, Luisi BF. 2009. Crystal structure of *Escherichia coli* polynucleotide phosphorylase core bound to RNase E, RNA and manganese: Implications for catalytic mechanism and RNA degradosome assembly. *J Mol Biol* **389:** 17–33.

Okabe Y, Sano T, Nagata S. 2009. Regulation of the innate immune response by threonine-phosphatase of Eyes absent. *Nature* **460:** 520–524.

Otwinowski Z, Minor W. 1997. Processing of X-ray diffraction data collected in oscillation mode. *Methods Enzymol* **276:** 307–326.

Parrish JZ, Xue D. 2003. Functional genomic analysis of apoptotic DNA degradation in *C. elegans*. *Mol Cell* **11:** 987–996.

Potterton E, Briggs P, Turkenburg M, Dodson E. 2003. A graphical user interface to the CCP4 program suite. *Acta Crystallogr D Biol Crystallogr* **59:** 1131–1137.

Raijmakers R, Schilders G, Pruijn GJ. 2004. The exosome, a molecular machine for controlled RNA degradation in both nucleus and cytoplasm. *Eur J Cell Biol* **83:** 175–183.

Reichlin M, Maddison PJ, Targoff I, Bunch T, Arnett F, Sharp G, Treadwell E, Tan EM. 1984. Antibodies to a nuclear/nucleolar antigen in patients with polymyositis overlap syndromes. *J Clin Immunol* **4:** 40–44.

Schaeffer D, Tsanova B, Barbas A, Reis FP, Dastidar EG, Sanchez-Rotunno M, Arraiano CM, van Hoof A. 2009. The exosome contains domains with specific endoribonuclease, exoribonuclease and cytoplasmic mRNA decay activities. *Nat Struct Mol Biol* **16:** 56–62.

Schuck P. 2000. Size-distribution analysis of macromolecules by sedimentation velocity ultracentrifugation and lamm equation modeling. *Biophys J* **78:** 1606–1619.

Shi Z, Yang WZ, Lin-Chao S, Chak KF, Yuan HS. 2008. Crystal structure of *Escherichia coli* PNPase: Central channel residues are involved in processive RNA degradation. *RNA* **14:** 2361–2371.

Suzuki N, Noguchi E, Nakashima N, Oki M, Ohba T, Tartakoff A, Ohishi M, Nishimoto T. 2001. The *Saccharomyces cerevisiae* small GTPase, Gsp1p/Ran, is involved in 3′ processing of 7S-to-5.8S rRNA and in degradation of the excised 5′-A0 fragment of 35S pre-rRNA, both of which are carried out by the exosome. *Genetics* **158:** 613–625.

Symmons MF, Jones GH, Luisi BF. 2000. A duplicated fold is the structural basis for polynucleotide phosphorylase catalytic activity, processivity, and regulation. *Structure* **8:** 1215–1226.

Symmons MF, Williams MG, Luisi BF, Jones GH, Carpousis AJ. 2002. Running rings around RNA: A superfamily of phosphate-dependent RNases. *Trends Biochem Sci* **27:** 11–18.

Torchet C, Bousquet-Antonelli C, Milligan L, Thompson E, Kufel J, Tollervey D. 2002. Processing of 3′-extended read-through transcripts by the exosome can generate functional mRNAs. *Mol Cell* **9:** 1285–1296.

van Dijk EL, Schilders G, Pruijn GJ. 2007. Human cell growth requires a functional cytoplasmic exosome, which is involved in various mRNA decay pathways. *RNA* **13:** 1027–1035.

van Hoof A, Lennertz P, Parker R. 2000. Yeast exosome mutants accumulate 3′-extended polyadenylated forms of U4 small nuclear RNA and small nucleolar RNAs. *Mol Cell Biol* **20:** 441–452.

Wu CJ, Yang XF, McLaughlin S, Neuberg D, Canning C, Stein B, Alyea EP, Soiffer RJ, Dranoff G, Ritz J. 2000. Detection of a potent humoral response associated with immune-induced remission of chronic myelogenous leukemia. *J Clin Invest* **106:** 705–714.

Xie L-H, Sin FW-Y, Cheng SC-S, Cheung Y-K, Chan K-T, Xie Y, Xie Y. 2008. Activation of cytotoxic T lymphocytes against CML28-bearing tumors by dendritic cells transduced with a recombinant adeno-associated virus encoding the CML28 gene. *Cancer Immunol Immunother* **57:** 1029–1038.

Yang X-F, Wu CJ, Chen L, Alyea EP, Canning C, Kantoff P, Soiffer RJ, Dranoff G, Ritz J. 2002. CML28 is a broadly immunogenic antigen, which is overexpressed in tumor cells. *Cancer Res* **62:** 5517–5522.

Yasutomo K, Horiuchi K, Kagami T, Tsukamoto H, Hashimura C, Urushihara M, Kuroda Y. 2001. Mutation of DNASE1 in people with systemic lupus erythematosus. *Nat Genet* **28:** 313–314.

Yeates TO. 1997. Detecting and overcoming crystal twinning. *Methods Enzymol* **276:** 344–358.

Zhou H, Zhang D, Wang Y, Dai M, Zhang L, Liu W, Liu D, Tan H, Huang Z. 2006. Induction of CML28-specific cytotoxic T cell responses using co-transfected dendritic cells with CML28 DNA vaccine and SOCS1 small interfering RNA expression vector. *Biochem Biophys Res Commun* **347:** 200–207.

Downloaded from rnajournal.cshlp.org on April 26, 2024 - Published by Cold Spring Harbor Laboratory Press

Structural and biochemical characterization of CRN-5 and Rrp46: An exosome component participating in apoptotic DNA degradation

Che-Chuan Yang, Yi-Ting Wang, Yu-Yuan Hsiao, et al.

RNA 2010 16: 1748-1759 originally published online July 21, 2010
Access the most recent version at doi:10.1261/rna.2180810

Supplemental Material	**http://rnajournal.cshlp.org/content/suppl/2010/06/25/rna.2180810.DC1**
References	This article cites 60 articles, 19 of which can be accessed free at: **http://rnajournal.cshlp.org/content/16/9/1748.full.html#ref-list-1**
Open Access	Freely available online through the *RNA* Open Access option.
License	Freely available online through the RNA Open Access option.
Email Alerting Service	Receive free email alerts when new articles cite this article - sign up in the box at the top right corner of the article or **click here.**

To subscribe to *RNA* go to:
http://rnajournal.cshlp.org/subscriptions